nature food

ARTICLES

https://doi.org/10.1038/s43016-021-00282-0

Check for updates

Pollen-inspired enzymatic microparticles to reduce organophosphate toxicity in managed pollinators

Jing Chen[1], James Webb[1], Kaavian Shariati[1], Shengbo Guo[2], Jin-Kim Montclare[2], Scott McArt[3] and Minglin Ma[1]✉

Pollinators support the production of the leading food crops worldwide. Organophosphates are a heavily used group of insecticides that pollinators can be exposed to, especially during crop pollination. Exposure to lethal or sublethal doses can impair fitness of wild and managed bees, risking pollination quality and food security. Here we report a low-cost, scalable in vivo detoxification strategy for organophosphate insecticides involving encapsulation of phosphotriesterase (OPT) in pollen-inspired microparticles (PIMs). We developed uniform and consumable PIMs capable of loading OPT at 90% efficiency and protecting OPT from degradation in the pH of a bee gut. Microcolonies of *Bombus impatiens* fed malathion-contaminated pollen patties demonstrated 100% survival when fed OPT–PIMs but 0% survival with OPT alone, or with plain sucrose within five and four days, respectively. Thus, the detrimental effects of malathion were eliminated when bees consumed OPT–PIMs. This design presents a versatile treatment that can be integrated into supplemental feeds such as pollen patties or dietary syrup for managed pollinators to reduce risk of organophosphate insecticides.

Pollinators provide vital pollination services to crops by facilitating fertilization and subsequent production of seeds and fruit. It is frequently cited that one-third of the food we consume is dependent on pollinators[1–3]. Both wild and managed pollinators are critical for ensuring pollination services; each contributes approximately equally to crop pollination[4,5]. However, wild and managed pollinators are currently experiencing declines in the form of range contractions, population declines and unsustainable hive losses.

Insecticide usage can cause unintended consequences by harming non-target organisms such as pollinators[6]. Exposure to insecticides is one of the key global drivers of declines in pollinator health[7]. A particular group of insecticides, organophosphates (OPs), have a market value of over US$7 billion and account for more than a third of insecticide sales worldwide. OPs exhibit high toxicity towards honeybees and bumblebees and are frequently exposed to pollinators[8–11]. OP insecticides influence insect cholinergic neural signalling through inhibition of carboxyl ester hydrolases, particularly acetylcholinesterase (AChE) which breaks down acetylcholine. OPs inactivate AChE through irreversible covalent inhibition, causing a build-up of acetylcholine and overstimulation of nicotinic and muscarinic receptors[12,13]. Malathion and parathion are the two of the most widely applied OPs in commercially pollinated crops[14]. Malaoxon, malathion's metabolite, is 1,000-fold stronger at inhibiting AChE than malathion[15]. Malathion and parathion exhibit oral median lethal dose (LD_{50}) values of 0.38 and 0.175 µg per bee, respectively[16].

Phosphotriesterases are metalloenzymes that hydrolyse the triester linkage found in OP insecticides[17]. There are several variants of phosphotriesterase; the most frequently used, amidohydrolase phosphotriesterase (OPT), is isolated from bacteria *Pseudomonas diminuta* or *Flavobacterium* ATCC 27551 and exhibits a triose phosphate isomerase (TIM)-barrel fold structure[18,19]. OPT can be easily produced from transfected *Escherichia coli* culture with the appropriate OPT plasmid sequence[20,21]. OPT has a wide substrate specificity; it exhibits optimal hydrolysis on encountering paraoxon (parathion's metabolite) at a rate approaching the limit of diffusion[22]. OPT performs best by hydrolysing substrates that possess phenol leaving groups, yet it will also successfully degrade thiol linkages as in the case of malathion[23,24]. Previously, OPT has been considered in a bioremediation capacity to detoxify heavily contaminated soils, as well as a treatment for OP-insecticide or nerve-agent poisoning[25–27]. However, OPT application has demonstrated poor efficacy in industry due to its poor stability at a low pH and high temperatures[28]. Bioactivity rapidly declines at pH <8.0. At pH 7.0, activity is less than half of its maximum potential. At the optimum pH range of 8.0–9.5, the Co^{2+}–OPT complex maintains thermostability below 45 °C; above 45 °C, the stability rapidly declines until deactivation at 60 °C (ref. [29]). Efforts to improve stability and function have focused on engineering OPT via rational design[30–33], directed evolution[20] and the incorporation of non-canonical amino acids[28,34].

In this Article, we report a biomaterial approach to control organophosphate toxicity aimed at managed bees (that is, bumblebees such as the common eastern bumblebee, *Bombus impatiens*, or the western honeybee, *Apis mellifera*) using OPT-loaded microparticles (Fig. 1). We used *B. impatiens* for our in vivo assays, although a similar gut pH exists for *A. mellifera*[35,36], thus our results may be relevant to *A. mellifera* as well. We chose calcium carbonate microparticles to deliver OPT on the basis of several design considerations. First, the microparticles mimic pollen grains in size and are therefore easily consumed by bees. Both bumblebees and honeybees have a gastrointestinal (GI) tract composed of a crop and ventriculus separated by a proventricular valve which

[1]Department of Biological and Environmental Engineering, Cornell University, Ithaca, NY, USA. [2]Department of Chemical and Biomolecular Engineering, New York University Tandon School of Engineering, Brooklyn, NY, USA. [3]Department of Entomology, Cornell University, Ithaca, NY, USA.
✉e-mail: mm826@cornell.edu

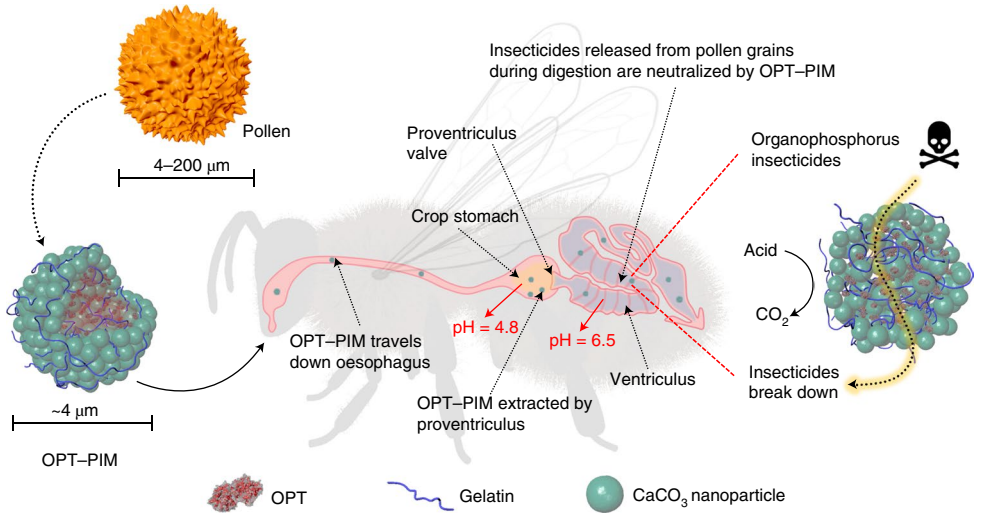

Fig. 1 | A schematic of the passage of microparticles through a bee digestive tract. Microparticles analogous to pollen grains move into the midgut as they are extracted by the proventriculus, which draws particulates out of the crop stomach. The PIM structure protects the encapsulated protein from gastric acidity. PIMs are retained in the midgut to detoxify pesticides as they are released during pollen digestion.

mechanistically extracts micro-sized particles for digestion[37]. Second, by harnessing the acid scavenging capability of $CaCO_3$, the microparticles can protect OPT from unfavourable acidic GI conditions to maintain enzyme bioactivity once they are consumed by bees. The pH of the crop and ventriculus are 4.8 and 6.5, respectively[36–38], well below the optimal pH conditions of OPT[29]. Third, $CaCO_3$ microparticles (2–50 μm) are relatively easy and inexpensive to produce in large quantities and are capable of loading biomacromolecules during production[39]. With optimized fabrication parameters and, importantly, the inclusion of gelatin as an additive, we produced homogenously sized microparticles that encapsulated OPT at ~90% efficiency and displayed a superior suspension stability in sucrose. In vitro studies confirmed the protective effect of the microparticles on OPT bioactivity. The OPT-encapsulated pollen-inspired microparticles (OPT–PIMs) allowed 100% survival of microcolonies of bees fed malathion-contaminated pollen patties, while 0% survival was observed for those fed with OPT alone or plain sucrose after 5 and 4 days, respectively. To understand the protective properties and stability of PIMs, we fed bees PIMs loaded with a FITC-labelled protein, human serum albumin (HSA–PIMs). Fluorescent imaging confirmed almost complete extraction of PIMs out of the crop stomach by 1 h and their stability throughout digestion for 12 h. This versatile, scalable, low-cost detoxification strategy can act as a precautionary or remedial measure for managed pollinators when pollinating in areas of organophosphate application, to address the issue of pollinator exposures.

Results and discussion

Characterizations of PIMs. Calcium carbonate microparticles can be easily fabricated by rapidly mixing equimolar 0.33 M solutions of $CaCl_2$ and Na_2CO_3. Size and shape can be acutely controlled by altering synthesis parameters such as stirring speed, time and additive inclusion[40,41]. Initially, we fabricated $CaCO_3$ microparticles with no inclusion of an additive, nor control of stirring time. The product displayed high incidences of aggregation, calcite crystal growth and poor size homogeneity (Fig. 2a); the average diameter was around 8.2 ± 5.7 μm with a large size distribution under pH 7.4, which caused poor suspension stability. To circumvent these challenges, we restricted stirring time to 10 s and included gelatin (24 mg ml^{-1}) as an additive, which resulted in smaller and consistently homogenously sized (3.9 ± 0.7 μm) microparticles. Gelatin was chosen because it is an easily obtained, low-cost natural additive. It is reported that the zeta potential of gelatin is −13.2 mV (ref. [42]) and it could thus interact with Ca^{2+} to form a gelatin–Ca complex that acts as a nucleation agent, subsequently enhancing microparticle stability. Given that these microparticles can be digested by bees in similar ways to pollen grains, we refer to them as pollen-inspired microparticles or PIMs (Fig. 2b). PIMs displayed a superior suspension stability in sucrose. The significantly improved suspension stability was confirmed using a biophotometer that measured the uppermost layer of the microparticle suspension. After 2 d, ~90% of unmodified microparticles had settled while >75% of PIMs maintained good suspension stability. PIMs took 6 d to fully settle, whereas unmodified microparticles only took 3 d (Fig. 2c). The sucrose media used to suspend the microparticles was at a typical concentration used to feed wintering honeybees (2 g ml^{-1}). Although the molecular mechanism behind crystal growth and aggregation is unclear[43], scanning electron microscope (SEM) imaging confirmed that the gelatin-modified microparticles maintained a highly porous nanoparticle aggregation structure (Fig. 2f). Nanometre-size pores are known to provide accessible channels for biomacromolecule diffusion and a high internal surface area to allow physical adsorption with high substrate loading[44].

Since OPT–PIMs need to maintain function when passing through acidity presented by the crop stomach, we tested the PIM stability in pH 4.8 for 30 min. PIMs at pH 4.8 displayed a fractional shift to a smaller size distribution (3.4 ± 0.6 μm) (Fig. 2b). When the test was extended to 1.5 h, the PIMs still largely retained their shape, although the average particle size further decreased to 1.4 ± 0.4 μm (Supplementary Fig. 1). We then repeated our PIM fabrication process using high reagent volumes to demonstrate the capacity for large-scale manufacture. PIMs were successfully produced at a 1 l total volume (Fig. 2d) and displayed a size distribution comparable to that of PIMs fabricated at small scale, with an average size of 4.3 ± 1.4 μm (Fig. 2e). Microparticle pore size was analysed in accordance with density functional theory using N_2 adsorption isotherms. PIM nanochannel volumes dropped from 0.0067 to 0.0043 $cm^3 g^{-1}$ following HSA encapsulation, which further confirmed protein loading (Fig. 2g). Nanochannel diameters only dropped from 14 to 12 nm, which indicated that protein loading did not block channels and would still permit OPs to enter for enzymatic degradation.

In vitro degradation of organophosphate pesticides with OPT–PIMs. Protein loading and gelatin modification of PIMs was further confirmed through confocal laser scanning microscopy. HSA was

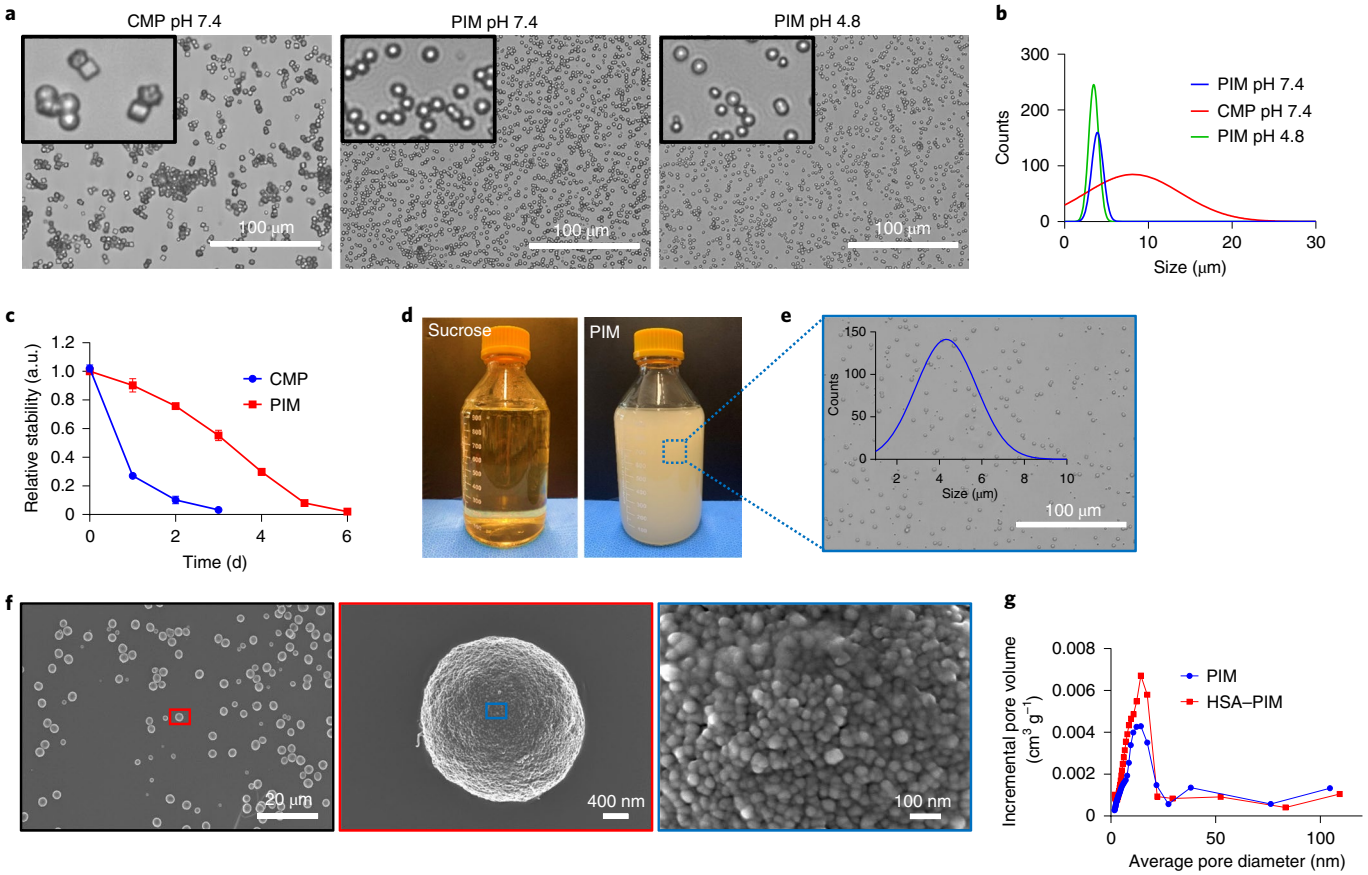

Fig. 2 | Characterizations of the stability, size distribution and morphology of PIMs. a, Morphological analysis of unmodified $CaCO_3$ microparticles (control) in pH 7.4 and PIMs in pH 7.4 and 4.8. (CMP denotes unmodified $CaCO_3$ microparticles, included as the control.) Optical microscope images are shown and insets are higher magnifications. **b**, Size distribution analysis of PIMs and unmodified microparticles in pH 7.4 and PIMs in pH 7.4 and 4.8. **c**, Relative suspension stability of unmodified microparticles and PIMs in 2 g ml^{-1} sucrose. **d**, Large-scale fabrication of PIMs. **e**, Morphological analysis and size distribution analysis of PIMs fabricated at a large scale. **f**, SEM imaging of microparticles to determine PIM surface morphology. **g**, Pore size distribution analysis of PIMs and PIMs loaded with HSA. Data are presented as means and error bars represent the standard deviation.

used in this instance as a model protein. Microparticles exhibited an overlay of Cy5.5-conjugated gelatin and FITC-conjugated HSA (FITC–HSA) in the full morphology of each microparticle (Fig. 3a). The confocal laser scanning microscopy (CLSM) imaging indicated gelatin conjugation and protein loading throughout the microparticle volume. The protein loading efficiency (PLE, percentage of protein loaded inside the microparticles relative to the total amount of protein added), as characterized spectrophotometrically using the FITC–HSA, varied as a function of the protein feeding content (PFC, percentage of the total amount of protein added relative to the total mass of the protein and microparticles). From the PLE and PFC, we also calculated the protein loading capacity (PLC, the total entrapped amount of protein divided by the total mass of the protein-loaded microparticles). HSA–PIMs presented a high PLE of 85.5% (PLC = 4.31%) for gelatin-modified PIMs and 83.6% (PLC = 4.21%) for unmodified microparticles at 5% PFC (Fig. 3b), consistent with previous studies[39]. The loading efficiency decreased as the PFC increased. For PIMs, a PLE of 67.1% (PLC = 6.94%) was obtained at 10% PFC, and a PLE of 52.1% (PLC = 8.42%) was obtained at 15% PFC. In the case of unmodified microparticles, a PLE of 64.1% (PLC = 6.65%) and a PLE of 47.1% (PLC = 7.67%) were obtained, respectively (Fig. 3b). Considering the loading efficiency decrease at higher PFCs and the intrinsic value of OPT, we selected 5% as a baseline to test OPT loading in PIMs. OPT presented 88.1% PLE (PLC = 4.43%) at 5% PFC and 90.1% PLE (PLC = 1.81%) at 2% PFC (Fig. 3c). We found that a concentration of 0.5 mg ml^{-1} OPT was sufficient to initiate rapid hydrolysis of methyl paraoxon to visibly form nitrophenol (Supplementary Fig. 2). A 2% PFC yielded an OPT concentration of 1.21 mg ml^{-1} in OPT–PIMs, which could be further diluted to 0.5 mg ml^{-1}; we found this dilution offered adequate sucrose to render the solution sufficiently attractive to bumblebees for consumption. Furthermore, it was evaluated that no protein was released from the PIMs up to 7 d following fabrication while suspended in 2 g ml^{-1} sucrose (Supplementary Fig. 3).

Previous studies have shown that OPT catalytic efficiency and conformational stability can vary on structural mutagenesis and variation in the central metal cation[30,45,46]. In our experimentation, we used wild-type Co^{2+}-bound phosphotriesterase (molecular weight 39 kDa) (Supplementary Fig. 4), which is the optimum metalloenzyme complex capable of a K_{cat} K_m^{-1} of 7.6×10^7 M^{-1} s^{-1} in hydrolysing paraoxon, where K_{cat} is the turnover number and describes how many substrate molecules are transformed into products per unit time by a single enzyme, and K_m gives a description of the affinity of the substrate to the active site of the enzyme. For the successful function of our design, it is critical that OPT–PIMs are able to maintain bioactivity in the conditions of a bee digestive tract (pH 4.8 in the crop stomach). Therefore, bioactivity and enzyme stability of OPT–PIMs and free OPT were assessed in vitro over a pH range using OPT 0.5 mg ml^{-1} and either 0.5 mM paraoxon or 0.44 mM malathion. Paraoxon assays were carried out by measuring the absorbance of nitrophenol as it is produced from the OPT-catalysed degradation of paraoxon. The relative

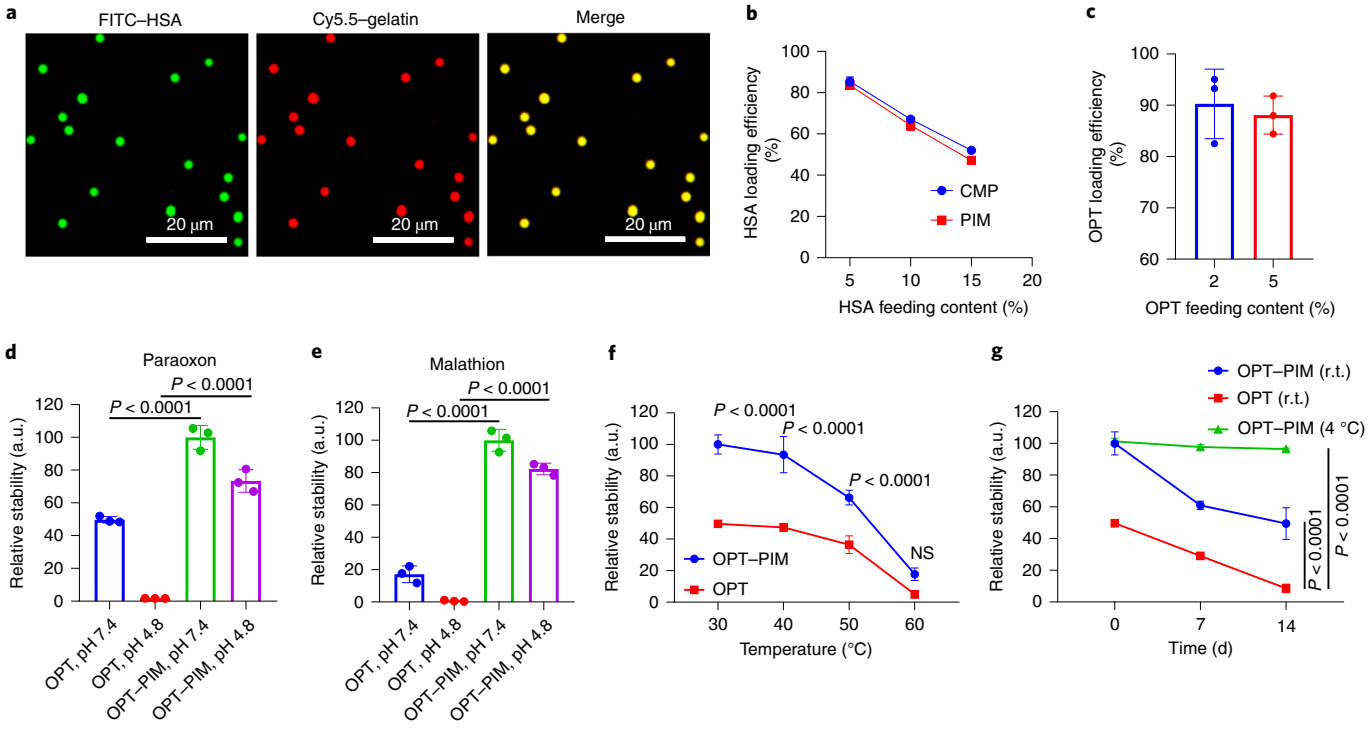

Fig. 3 | Characterizations of OPT encapsulation and activity in PIMs. a, Fluorescent imaging of PIMs containing Cy5.5-modified gelatin and FITC-conjugated HSA. **b**, PLE of CMP and PIM loaded with HSA at 5, 10 and 15% PFC. **c**, PLE of PIM loaded with OPT at 2% and 5% PFC. **d**, Relative activity of OPT–PIM and free OPT in paraoxon hydrolysis under pH 7.4 and 4.8 ($n=3$). **e**, Relative activity of OPT–PIM and free OPT in malathion hydrolysis under pH 7.4 and 4.8 ($n=3$). **f**, Temperature-dependent relative activity of OPT–PIM and free OPT in paraoxon hydrolysis when incubated at temperatures 30, 40, 50 and 60 °C ($n=3$). **g**, Long-term relative activity of OPT–PIM and free OPT in paraoxon hydrolysis when stored at room temperature and 4 °C ($n=3$). Statistical analysis was performed by using one-way ANOVA tests (**d**, **e**) and two-way ANOVA tests (**f**, **g**). Data are presented as means and error bars represent the standard deviation. NS, no statistical significance; r.t., room temperature.

enzymatic activity was obtained by normalizing the absorbances of both free OPT and OPT–PIMs to that of OPT–PIMs incubated at pH 7.4. As shown in Fig. 3d, free OPT yielded an activity of 49.7%, approximately half that of OPT–PIMs at pH 7.4. Meanwhile, the K_m was determined to be 1.83 mM for OPT–PIMs, lower than that of free OPT (4.80 mM) in 2 g ml^{-1} sucrose (Supplementary Fig. 5). The maximum velocity (V_{max}) of OPT–PIMs (0.45 mM min^{-1}) was approximately three times that of free OPT (0.13 mM min^{-1}). We suspect that the higher performance of OPT–PIMs occurs because microparticle encapsulation facilitates enhanced enzyme kinetics[47–49]. In addition, we anticipated the $CaCO_3$ element of the microparticle structure would bear an 'acid scavenging' ability, which could neutralize acid in the microparticle's immediate vicinity, allowing encapsulated OPT to outperform free enzyme in acidic conditions[50]. As expected, OPT–PIMs at pH 4.8 displayed lower activity (73.4%) than that at pH 7.4. However, free enzyme assays almost did not function at all (1.7%) at pH 4.8.

An absorbance from malathion hydrolysis was characterized using Ellman's reagent (5,5′-dithiobis-2-nitrobenzoic acid or DTNB), which can react with the thiol group of malathion's breakdown product to form 2-nitro-5-thiobenzoate or TNB^{2-}, which has an absorbance at 412 nm (Supplementary Fig. 6). In malathion degradation assays, a similar trend could be detected at both pH 7.4 and pH 4.8. OPT is less adept at cleaving thiol groups, and therefore enzymatic degradation of malathion is relatively slow. Free OPT therefore displayed much a lower activity of 17.1% at pH 7.4 and 0.6% at pH 4.8 (Fig. 3e). However, OPT–PIMs could still maintain high activity of 82.2% at pH 4.8. This indicates that the benefits of the microparticle design are more pronounced when degrading OPs because OPT can degrade relatively slowly. The superior catalytic performance of PIMs in pH 4.8 demonstrates the importance of utilizing a biomaterial element to protect enzyme catalysts in oral consumption.

We wished to understand the stability of our system under significant thermal stress, as any treatment could experience high summer temperatures when administered to bees. OPT has been found to denature at temperatures exceeding 45 °C. We aimed to determine whether microparticle encapsulation offers any protection from thermal denaturation. We tested the capacity for the microparticle design to withstand elevated temperatures by measuring paraoxon breakdown following enzyme incubation at temperatures ranging from 30 to 60 °C. The relative enzymatic activity was obtained by normalizing the absorbances of both free OPT and OPT–PIMs to that of OPT–PIMs incubated under 30 °C. As shown in Fig. 3f, free OPT displayed half the bioactivity of OPT–PIMs under 30 °C. The enzymatic activity of free OPT dramatically dropped to 36.5% after incubation at 50 °C, whereas the activity of OPT–PIMs remained at 66.3% at the same temperature. Further, increases in temperature ≥60 °C resulted in little catalytic activity (5.0%) of the free enzyme, which is much lower than that of OPT–PIMs (17.7%). We found that OPT maintained greater bioactivity when encapsulated in PIMs relative to the case of free OPT as temperatures increased. This is important for the potential application of our design, as it may be administered at elevated temperatures.

To gauge the time taken for treatment to lose functionality, bioactivity of each group treatment relative to OPT–PIMs was measured over time when kept at room temperature (25 °C). Microparticle activity maintained around 60% of original activity after 7 d and 49.5% after 14 d, whereas free enzyme activity reduced to ~30% and <10%, respectively. OPT–PIMs stored at 4 °C maintained almost

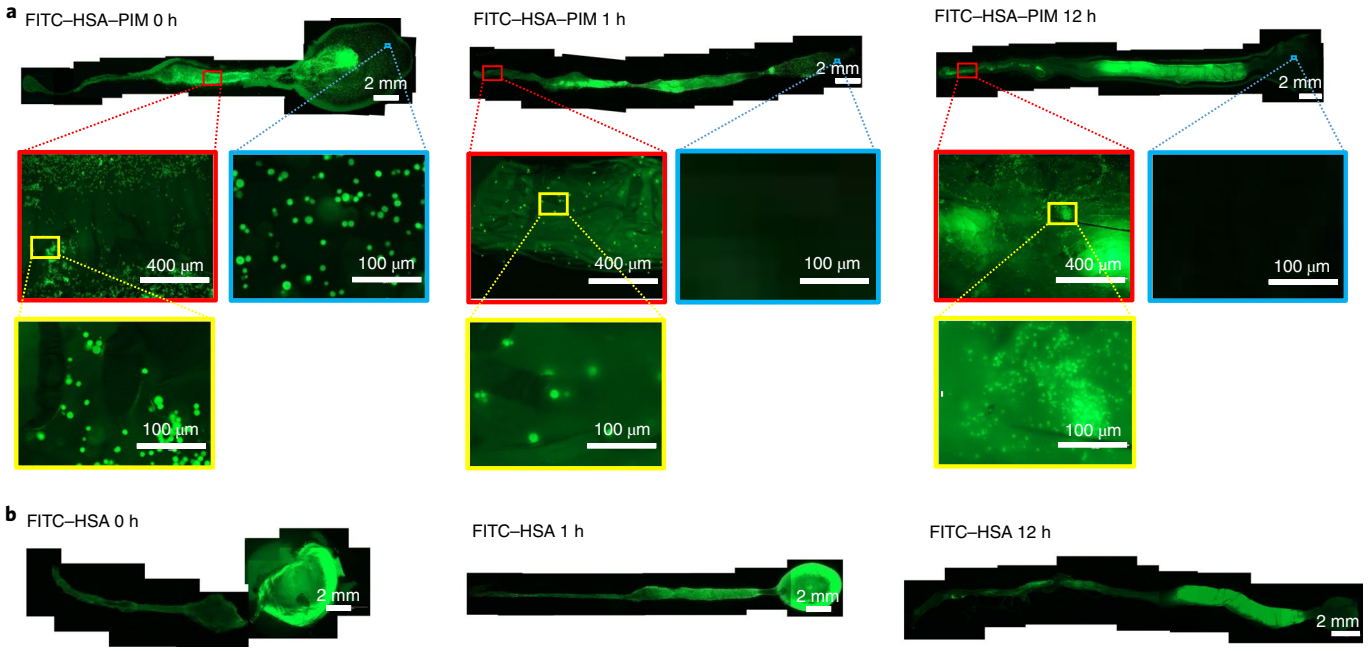

Fig. 4 | Tracking of digested PIMs by fluorescent imaging of bumblebee GI tracts. a, GI tracts following HSA–PIM treatment; fluorescence was maintained up to 12 h post-consumption. Microparticle morphology was clearly visible and microparticles were successfully drawn into the midgut ($n = 3$; relatively brighter background at 1 and 12 h was probably due to protein leakage during digestion). **b**, GI tracts following free-HSA treatment ($n = 3$).

100% activity after 14 d (Fig. 3g). The microparticle's capacity for long-term bioactivity and protein sequestration indicates a practical shelf life of the design. Other enzyme-engineering efforts such as genetic engineering of the catalytic and binding pockets, introducing additional chemical functionalities, such as disulfide bridges or fluorine moieties, or incorporation of additives such as sugars, polyols, detergents, polymers and amino acids may improve the catalytic efficiency of OPT and further enhance its storage stability[51].

In vivo characterizations of PIMs. *B. impatiens* were used for in vivo experimentation because colonies can be maintained indoors during the winter in a practical and accessible box. Bumblebees have displayed a susceptibility to OPs comparable to *A. mellifera*[52]. To understand the retention performance of PIMs once consumed, we fed bumblebees microparticles loaded with FITC-labelled HSA (FITC–HSA–PIMs) and free FITC–HSA for 30 min, before extracting digestive tracts over a 12 h period for fluorescent microscopy analysis (Fig. 4). FITC displayed PIMs successfully in the crop stomach and ventriculus sections of the GI tract for samples collected at 0, 1, 4 and 12 h. During the first hour of digestion, microparticles were distributed across both the crop stomach and ventriculus. By 1 h, the majority of microparticles had travelled out of the crop stomach, before clearance into the ventriculus, suggesting proventricular filtering of PIMs (Fig. 4a). By 12 h, no PIMs were observable in the crop stomach, comparable to background autofluorescence of untreated bee (Supplementary Fig. 7), but a significant number of PIMs were still detected in the posterior section of the GI tract. In case of free FITC–HSA, most of the fluorescence was located in the ventriculus at 4 h, while a large amount was observed in crop stomach at 1 h (Fig. 4b). The data suggest that PIMs are digested akin to pollen grains, increasing the number of microparticles drawn into the ventriculus alongside pollen. This maximizes PIM function in detoxifying pollen as it is digested. This is significant because OPs are often found in high quantities in pollen, which may be held in the posterior section of the ventriculus for digestion for up to 12 h or more[37,53]. We were not able to quantify the degree of fluorescence because FITC fluorescence is pH dependent[54]; the presence of microparticles would have altered stomach pH to the point where fluorescence readings would have been inaccurate. However, these images qualitatively suggest that the PIM design improved retention and provided protection from the denaturation of loaded proteins.

Efficacy and survival studies. We were able to further validate our characterization of OPT–PIM efficacy via quantification of AChE activity when mixed with our treatment and paraoxon. As AChE is inhibited by OPs such as paraoxon, high AChE activity would indicate effective detoxification through our treatment. Acetylthiocholine cleavage via AChE can be used to quantify AChE activity, as the thiocholine product reacts with DTNB to form TNB^{2-}, which has an absorbance at 412 nm (Fig. 5a). Homogenized honeybee cells were able to maintain 91.5% of AChE activity when treated with 0.5 mM paraoxon and OPT–PIMs, relative to the positive control (homogenized honeybee cells without any paraoxon treatment). This was a stark improvement in AChE functionality relative to the negative control (homogenized honeybee cells treated with paraoxon but no free OPT or OPT–PIMs treatment), which resulted in a relative activity reduction of ~72%. Samples treated with free OPT retained 18.8% less activity than that of samples treated with OPT–PIMs (Fig. 5b).

Groups of 50 bumblebees were treated with paraoxon or malathion-contaminated pollen balls and OPT–sucrose treatments to determine the efficacy of treatments in reducing mortality under OP exposure (Fig. 5c). Paraoxon and malathion present oral LD_{50}s for honeybees at 0.0175 and 0.38 µg per bee, respectively[55]. This data set a benchmark for OP doses we would attempt to administer and subsequently detoxify to demonstrate OPT–PIM efficacy. Bumblebees consume approximately 40.5 µg pollen per day depending on body mass[56]. Based on this figure, we initially formed pollen balls containing 0.432 µg g^{-1} paraoxon and 9.383 µg g^{-1} malathion to feed without enzyme treatment as a negative control. We found these pollen balls caused no health deterioration after one week.

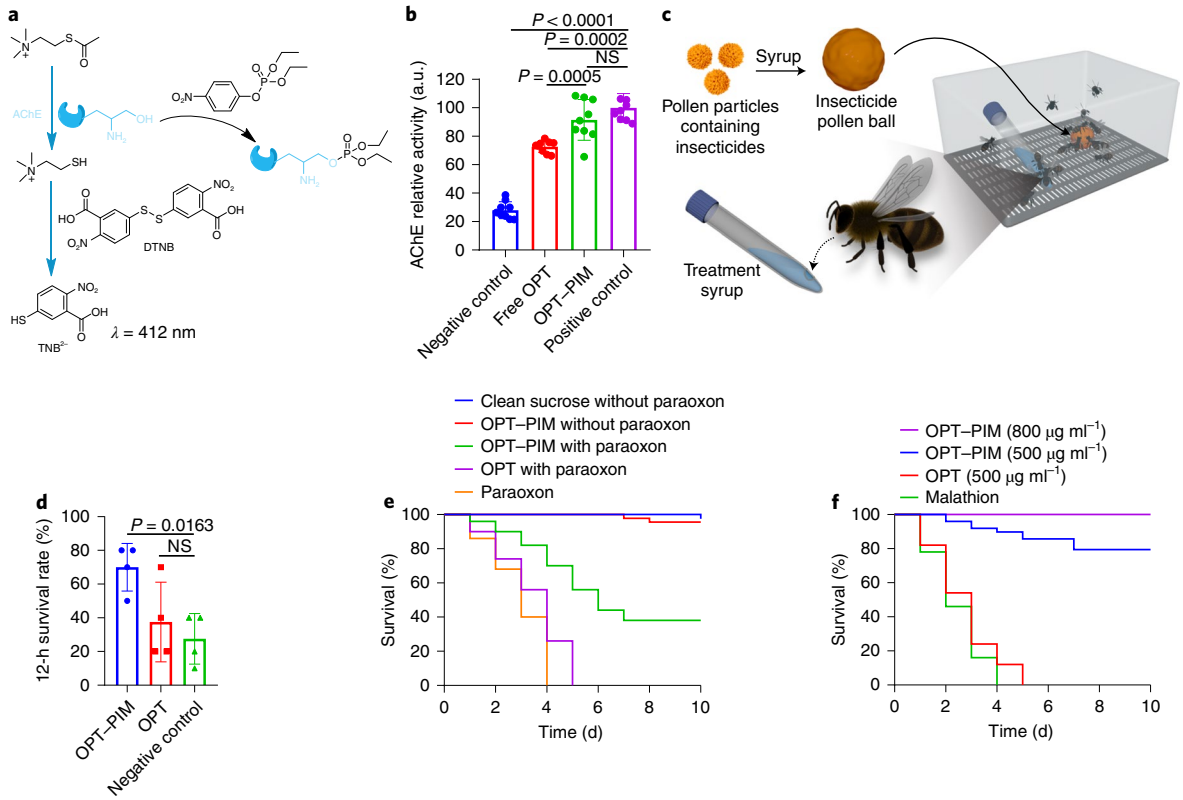

Fig. 5 | Characterization of OPT–PIM efficacy through AChE activity assay and bee survival experiments. a, The formation of thiocholine from acetylthiocholine through AChE cleavage can be characterized using DTNB. DTNB and thiocholine react to form TNB^{2-}, the absorbance of which can be measured at 412 nm. **b**, Relative activity of AChE from homogenized honeybees when incubated in 0.5 mM paraoxon or DI water (the positive control) and treated with samples of free OPT, OPT–PIM and DI water (the negative control). For this experiment, $n = 9$. The positive control is homogenized honeybee cells without any paraoxon treatment; the negative control is homogenized honeybee cells treated with paraoxon but no free OPT or OPT–PIMs treatment. **c**, The apparatus for determining mortality following contaminated pollen ball consumption against PIM treatment in syrup. **d**, The survival rate of bumblebees following acute exposure to paraoxon (50 μg g^{-1} pollen) over 12 h when treated with 500 μg ml^{-1} OPT treatments ($n = 40$). **e**, Exposure to paraoxon (15 μg g^{-1} pollen) over 10 d ($n = 50$). **f**, Exposure to malathion (750 μg g^{-1} pollen) over 10 d ($n = 50$). Statistical analysis was performed by using one-way ANOVA tests (**b**, **d**). Data are presented as means and error bars represent the standard deviation.

Subsequently, through trial and error, we significantly increased contamination to concentrations which caused significant mortality. We tested pollen balls containing 50 μg g^{-1} paraoxon over 12 h to measure the OPT–PIM impact against acute exposure. In this trial, OPT–PIMs at 500 μg ml^{-1} of OPT were able to maintain a 70% survival rate, whereas free enzyme- and sucrose-treated groups sustained 62.5 and 72.5% fatalities, respectively (Fig. 5d). Although OPT–PIMs largely detoxified acute exposure, the catalytic efficiency was not able to fully mitigate mortality.

A moderate level of toxicity was tested using 15 μg g^{-1} paraoxon- and 750 μg g^{-1} malathion-contaminated pollen balls against 50 μg ml^{-1} OPT treatments. Free OPT and no treatment resulted in 100% mortality after 5 and 4 d, respectively, following paraoxon toxicity. OPT–PIMs were able to maintain a slower incidence of mortality relative to other treatments. After 10 d, 38% of the group sample had survived. Groups containing non-contaminated pollen balls and either pure sucrose or PIM–sucrose maintained 100% and 96% survival, respectively. It is expected to see some minor mortality in any sample after 10 d (Fig. 5e). In malathion contaminated samples, OPT–PIM at 800 μg ml^{-1} of OPT was able to maintain 100% survival for the duration of observation, a lower concentration of 500 μg ml^{-1} maintained above 80% survival over 10 d. Free OPT- and sucrose-treated groups presented 100% mortality after 5 and 4 d, respectively, analogous to the paraoxon trial (Fig. 5f). We suspect the poor performance of free, unprotected OPT is in part driven by its higher denaturation in the acidic conditions of the digestive tract. Pollen grains release their internal contents as they progress along the midgut[57,58]. We assume that any OPs absorbed into pollen grains during incubation are also made available at this stage of digestion. This means that for the effective detoxification of contaminated pollen, OPT must retain bioactivity until it makes passage into the ventriculus. In addition, it is critical that a high concentration of OPT is drawn into the midgut to intercept paraoxon or malathion as pollen is digested. Both of these conditions have been facilitated via OPT encapsulation in PIMs.

Conclusions

Experimentation has shown that PIMs are able to enhance the bioactivity of OPT. OPT–PIMs outperform free OPT when tested under unfavourable conditions of temperature, storage and pH. The microparticle design has rendered OPT suitable for use in addressing pollinator OP intoxication, as it bestows functionality in gastric acidity and can maintain performance for longer durations, under elevated thermal stress. The microparticle design has also improved the functionality of OPT during digestion by considering the bee's digestive system. Microparticles are extracted into the midgut and retained for a long duration. The aforementioned advantages ultimately result in a lower rate of mortality when treated with OPT–PIM relative to free OPT. The benefits are most appreciable when degrading OPs, which are typically hydrolysed at a lower relative

rate (as in the case of malathion). This work has produced a viable product to mitigate insecticide damage to pollinator colonies and revealed new ways in which research can address the impacts of insecticide application through improving this current design, or by exploring new microparticle treatments.

Further research is required to determine the impact of the design on a colony as a whole in colony-scale testing. A characterization of how microparticles are distributed around colony castes and brood chambers when administered would give an indication of the potential of the design at a colony level. Emphasis should also be placed on testing the effect on pollination efficiency of crops, to comprehend the economic potential of the design if applied for agricultural purposes. Lastly, the relative enzymatic activity of dried and rehydrated OPT–PIMs was 56.6% that of OPT–PIMs without drying, suggesting that it may be feasible to treat wild pollinators. However, future work is needed to improve the effect of drying and rehydration on the enzyme activity, as well as study the differences in diets and feeding mechanisms between crop pests and beneficial insects. With more research, OPT–PIMs could potentially be administered in suitable feeding carriers in areas of intensive agriculture to exclusively reach pollinators and other non-target organisms.

Methods

Materials. NaCl, $CaCl_2$, Na_2CO_3, $CoCl_2$, KCl, Tris·HCl, DTNB, acetylthiocholine, imidazole, glycerol, nitrilotriacetic acid (NTA)-nickel beads, paraoxon, malaoxon, gelatin from porcine skin and HSA, ampicillin, chloramphenicol and isopropyl-β-D-1-thiogalactopyranoside (IPTG) were purchased from Sigma-Aldrich. Sugar was purchased from Domino Foods. The bicinchoninic acid (BCA) protein assay kit, Cy5.5-NHS and FITC–NHS were purchased from Thermo Fisher. *B. impatiens* were acquired from Biobest. *A. melifera* were acquired from colonies of the McArt Lab at Cornell. Bee pollen was acquired from CC Pollen.

OPT synthesis. Ampicillin, chloramphenicol and IPTG solutions were sterilized before use. *E. coli* bearing pQE30–PTE was cultured in Miller grade LB broth containing 100 μg ml^{-1} ampicillin and 25 μg ml^{-1} chloramphenicol at 37 °C. Once cultures in 5,000 ml flasks reached optical density (OD) 0.4, 500 μl $CoCl_2$ (1 M) was added, and at OD 0.8–1.0, 500 μl IPTG (200 mg ml^{-1}) was added for every litre of culture. The culture was left for a further 3 h before collecting. The culture was then centrifuged for 10 min at 1,333×*g* in 1 l centrifuge tubes, the supernatant was removed and the cell pellet was resuspended in 40 ml resuspension buffer (3.15 g Tris·HCl, 29.22 g NaCl, 56 g glycerol, 44 μl $CoCl_2$ (1 M), 144 mg imidazole, 1 l H_2O). The solution was then sonicated at 65% amplitude (5 s on, 25 s off) for 20 min in an ice bath. The solution was subsequently centrifuged for 1.5 h at 4,333×*g* and the supernatant collected as crude OPT. Crude OPT was purified using a histidine-select NTA-nickel bead affinity column. The column was equilibrated using an equilibration buffer (20 mM phosphate buffer, 300 mM NaCl, 10 mM imidazole) before crude OPT was run through the column and washed with further equilibration buffer. Captured OPT was then eluted with elution buffer (20 mM phosphate buffer, 300 mM NaCl, 250 mM imidazole). OPT was concentrated using Amicon Ultra 15 ml 3-kDa-membrane tubes and washed with saline three times. OPT concentration was determined using a BCA protein assay kit. Confirmation of OPT production was confirmed using SDS–PAGE.

OPT–PIM fabrication. In a 10 ml vial, 1 ml of each of the following was added in order and mixed continuously for 10 s using a magnetic stirrer at 6,000 r.p.m.: 24 mg ml^{-1} gelatin from porcine skin, OPT 3.364 mg ml^{-1} (5% PFC) or OPT 1.345 mg ml^{-1} (2% PFC), 0.33 M $CaCl_2$ and 0.33 M Na_2CO_3, to form OPT–PIMs. The solution was centrifuged at 1,000×*g* for 3 min and the supernatant subsequently removed. The remaining microparticles were suspended in either distilled water or 2 g ml^{-1} sucrose to form 0.5 mg ml^{-1} OPT. We carried out this experiment ten times through this project.

Microparticle morphology. Microparticle morphology was analysed by resuspending PIMs in 1 ml of distilled H_2O following centrifugation and analysing a drop of the solution under an EVOS FL microscope. To produce $CaCO_3$ microparticles to compare as a standard, the microparticle fabrication process was repeated without gelatin; distilled H_2O was added in substitute. Lyophilized microparticles were furthered analysed under SEM.

Microparticle size and pore size distribution. Microparticles were prepared as above; samples were either resuspended in pH 4.8, 0.1 M citric acid/sodium citrate buffer for 30 min (and 1.5 h) or resuspended as usual in deionized (DI) water. Samples were analysed under an EVOS FL microscope before size distribution analysis using ImageJ software. Pore size distribution was analysed by a Micromeritics ASAP 2460. This experiment was repeated three times.

Microparticle loading characterization. FITC–NHS was conjugated to HSA by an amide reaction and dialysis according to a previous report[59], followed by lyophilization. A standard curve of FITC–HSA was then prepared in the following concentrations: 2, 1.5, 1, 0.5, 0.25, 0.125, 0.625, 0.03125, 0 mg ml^{-1}. Microparticles were synthesized as described above using FITC–HSA in lieu of OPT at 15, 10 and 5% PFC (10.092, 6.724 and 3.364 mg ml^{-1}), in triplicate. Following centrifugation, the supernatant was collected and analysed together with standard curve samples using a Biotek Synergy 4 spectrophotometric plate reader at 490 nm to determine PLE. The process was repeated using OPT conjugated with FITC at 5 and 2% PFC. For microparticle fluorescent imaging, gelatin was conjugated to Cy5.5 with an amide reaction as previously mentioned, used as a substitute for regular gelatin and imaged under an EVOS FL microscope.

Protein-release testing. FITC–HSA loaded into PIMs and unmodified $CaCO_3$ microparticles were suspended in 2 g ml^{-1} sucrose, separated into multiple samples and placed on an orbital shaker at 400 r.p.m. A standard curve of FITC–HSA was made in previously mentioned concentrations, yet dissolved in sucrose. Every 24 h for 7 d, sample triplicates were centrifugated at 1,000×*g* for 5 min, before spectrophotometric analysis at 490 nm. Fluorescence readings were indicative of protein released from microparticles at each time point.

Kinetic study of OPT and OPT–PIMs. Paraoxon-ethyl was used as the substrate to perform enzyme kinetics measurements. OPT and OPT–PIMs were diluted to 0.5 mg ml^{-1} in 2 g ml^{-1} sucrose, and the substrate was dissolved in the same sucrose at a range of concentrations from 0.25 to 8 mM. To perform the test, 100 μl of the above OPT sample was added to a 96-well plate, followed by adding 100 μl substrate solution. On mixing, the absorption change at 405 nm was monitored using a plate reader (BioTek). The enzyme kinetics parameters were calculated using Michaelis–Menten kinetics.

Suspension stability. The same concentration of PIMs and non-modified microparticles were suspended in sucrose (2 g ml^{-1}) and separated into multiple samples of 10 ml volumes. One millilitre was taken from the upper layer of samples every 24 h for 7 d and analysed for optical density using an Eppendorf Biophotometer Plus at OD 600. Optical density values were indicative of microparticle concentration.

OPT–PIM pH stability. OPT–PIM was synthesized as previously described with 2% OPT feeding content. OPT–PIM and free OPT samples containing 0.5 mg ml^{-1} OPT were incubated in pH 4.8 citric acid/sodium citrate buffer or pH 7.4 PBS for 30 min. The pH of each buffer was confirmed using a VWR-B10P Symphony pH meter. Following incubation, 0.1 M NaOH was added to samples incubated at pH 4.8 to attain pH 7.4 for measurement. Standard curves of nitrophenol at concentrations 0.25, 0.125, 0.0613, 0.0313, 0.0156, 0.0062, 0.0031 and 0.0007 mg ml^{-1} were prepared in 2 mg ml^{-1} sucrose containing blank $CaCO_3$ microparticles at equal concentrations to that of OPT–PIM. A 100 μl volume of paraoxon at 0.5 mM and 100 μl of free OPT or OPT–PIM were added to a 96-well plate in triplicates following pH treatment. Enzyme activity was measured using a Biotek Synergy 4 spectrophotometric plate reader at 405 nm every 5 s for 2 min.

OPT–PIM thermal stability. OPT–PIMs were prepared as previously described, both OPT–PIMs samples and free OPT were diluted to 0.5 mg ml^{-1} OPT in 2 g ml^{-1} sucrose. Samples were incubated at 30, 40, 50 and 60 °C for 20 min before 100 μl of each sample and 100 μl 0.5 mM paraoxon were added to a 96-well plate in triplicate. Absorbance at 405 nm was measured spectrophotometrically as previously described[28,34] every 5 s for 2 min.

GI fluorescent imaging. Twenty-four bumblebees were individually placed in 4 oz, ventilated plastic cups and starved for 2 h. Bumblebees were subsequently fed FITC–HSA–PIM or free FITC–HSA in sucrose at 0.5 mg ml^{-1} HSA using 1.5 ml Eppendorf tubes, in triplicate. Following 30 min of feeding, treatments were removed and bumblebees from each treatment group were anesthetized after 0, 1, 4 and 12 h, and then immediately beheaded using dissection scissors. GI tracts were removed by cutting the perimeter of the abdomen before removing the crop and ventriculus and placing it on a glass slide. Samples were analysed for FITC fluorescence under an EVOS FL microscope.

AChE activity characterization. Honeybees were homogenized in 1x PBS and filtered using a 70 μm cell strainer. Honeybee cell membrane was diluted to 0.5 mg ml^{-1} protein concentration after analysis with a Pierce BCA protein assay kit. Samples of the filtrate with a 2 ml volume were combined with 1 ml 0.5 mg ml^{-1} OPT of OPT–PIMs, free OPT and DI water, followed by the addition of 1 ml 0.5 mM paraoxon or 1 ml DI water. AChE assays were performed in accordance with a previously described protocol[60]. An assay medium of 50 mM Tris·HCl, 20 mM KCl, 2 mM DTNB and 2 mM acetylthiocholine was prepared. A 100 μl volume of each experimental sample and 100 μl of the assay medium were added

in triplicate to a 96-well plate. Absorbance was measured at 412 nm in a Biotek Synergy 4 spectrophotometric plate reader every 30 s for 20 min. AChE activity was defined as the change of absorbance during the 20 min of reading.

Mortality testing. Pollen balls were prepared by mixing 5 ml of one of 3 OP conditions (malathion 1,500 μg ml^{-1}, paraoxon 100 μg ml^{-1}, paraoxon 30 μg ml^{-1}, distilled H_2O), with 10 g of high-desert bee pollen granules. The mixture was shaken until a homogeneous slurry was formed, then left at room temperature to allow full absorption of the OPs. The contaminated pollen was then crushed in a pestle and mortar. The mixture containing pollen and sucrose was rolled by hand into equally sized 3 g pollen balls. Treatments were prepared by diluting OPT–PIM and free OPT in sucrose (2 g ml^{-1}) to either 500 μg ml^{-1} or 800 μg ml^{-1} OPT. Groups of 50 bumblebees (*B. impatiens*) were placed in microcolony-rearing cages and treated with various combinations of either contaminated or non-contaminated pollen balls and one of the following: 500 μg ml^{-1} OPT–PIM sucrose, 800 μg ml^{-1} OPT–PIM sucrose, 500 μg ml^{-1} free OPT sucrose or pure sucrose. Each microcolony cage was given one pollen ball and 5 ml of OPT or plain sucrose solution provided in a centrifugal tube with a small aperture for feeding. Microcolonies were monitored every 12 h for mortalities until all bees had deceased or 10 d had elapsed. In the case of the acute mortality test, the trial was terminated after 12 h.

The effect of drying and rehydration on enzyme activity. OPT–PIMs were diluted to 500 μg ml^{-1} in water. Then 100 μl of OPT–PIMs was added to a 96-well plate and placed into vacuum oven over night until dry. A 100 μl volume of 2 g ml^{-1} sucrose was the added into each well and the whole plate was placed onto an orbital shaker for 10 min. After OPT–PIMs were fully suspended in sucrose, 100 μl of paraoxon was added to each well. On mixing, the absorption at 405 nm was monitored using a plate reader (BioTek). The relative enzymatic activity of rehydrated OPT–PIMs was 56.6% to that of OPT–PIMs without drying, suggesting that it may be feasible to treat wild pollinators despite room for improvement.

Statistical analysis. Data are presented as 'mean ± s.d.' as indicated in the figure legends. To determine statistical significance when comparing two groups, one-way or two-way analysis of variance (ANOVA) tests were used.

Reporting Summary. Further information on research design is available in the Nature Research Reporting Summary linked to this article.

Data availability

The data that support the findings of this study are available from the corresponding author on request. Source data are provided with this paper.

Received: 15 October 2020; Accepted: 20 April 2021;
Published online: 20 May 2021

References

1. Abernethy, V. D. Nature's services: societal dependence on natural ecosystems. *Popul. Environ.* **20**, 277–278 (1999).
2. Bartomeus, I. et al. Contribution of insect pollinators to crop yield and quality varies with agricultural intensification. *PeerJ* **2**, e328 (2014).
3. Klein, A. M. et al. Importance of pollinators in changing landscapes for world crops. *Proc. R. Soc. B* **274**, 303–313 (2007).
4. Kleijn, D. et al. Delivery of crop pollination services is an insufficient argument for wild pollinator conservation. *Nat. Commun.* **6**, 7414 (2015).
5. Reilly, J. R. et al. Crop production in the USA is frequently limited by a lack of pollinators. *Proc. R. Soc. B* **287**, 20200922 (2020).
6. Croft, B. A. *Arthropod Biological Control Agents and Pesticides* (Wiley, 1990).
7. Goulson, D., Nicholls, E., Botias, C. & Rotheray, E. L. Bee declines driven by combined stress from parasites, pesticides, and lack of flowers. *Science* **347**, 6229 (2015).
8. Rissato, S. R., Galhiane, M. S., de Almeida, M. V., Gerenutti, M. & Apon, B. M. Multiresidue determination of pesticides in honey samples by gas chromatography–mass spectrometry and application in environmental contamination. *Food Chem.* **101**, 1719–1726 (2007).
9. Ghini, S. et al. Occurrence and distribution of pesticides in the province of Bologna, Italy, using honeybees as bioindicators. *Arch. Environ. Contam. Toxicol.* **47**, 479–488 (2004).
10. Yao, J., Zhu, Y. C., Adamczyk, J. & Luttrell, R. Influences of acephate and mixtures with other commonly used pesticides on honey bee (*Apis mellifera*) survival and detoxification enzyme activities. *Comp. Biochem. Physiol. C* **209**, 9–17 (2018).
11. Sanchez-Bayo, F. & Goka, K. Pesticide residues and bees—a risk assessment. *PLoS ONE* **9**, e94482 (2014).
12. Peter, J. V., Sudarsan, T. I. & Moran, J. L. Clinical features of organophosphate poisoning: a review of different classification systems and approaches. *Indian J. Crit. Care Med.* **18**, 735–745 (2014).
13. Fukuto, T. R. Mechanism of action of organophosphorus and carbamate insecticides. *Environ. Health Perspect.* **87**, 245–254 (1990).
14. Lerro, C. C. et al. Organophosphate insecticide use and cancer incidence among spouses of pesticide applicators in the agricultural health study. *Occup. Environ. Med.* **72**, 736–744 (2015).
15. Rodriguez, O. P., Muth, G. W., Berkman, C. E., Kim, K. & Thompson, C. M. Inhibition of various cholinesterases with the enantiomers of malaoxon. *Bull. Environ. Contam. Toxicol.* **58**, 171–176 (1997).
16. Tomlin, C. *The Insecticide Manual: A World Compendium* (BCPC, 2009).
17. Pinjari, A. B., Pandey, J. P., Kamireddy, S. & Siddavattam, D. Expression and subcellular localization of organophosphate hydrolase in acephate-degrading *Pseudomonas* sp strain Ind01 and its use as a potential biocatalyst for elimination of organophosphate insecticides. *Lett. Appl. Microbiol.* **57**, 63–68 (2013).
18. Zheng, Y., Lan, W., Qiao, C., Mulchandani, A. & Chen, W. Decontamination of vegetables sprayed with organophosphate pesticides by organophosphorus hydrolase and carboxylesterase. *Appl. Biochem. Biotechnol.* **136**, 233–241 (2007).
19. Benning, M. M., Kuo, J. M., Raushel, F. M. & Holden, H. M. Three-dimensional structure of the binuclear metal center of phosphotriesterase. *Biochemistry* **34**, 7973–7978 (1995).
20. Roodveldt, C. & Tawfik, D. S. Directed evolution of phosphotriesterase from *Pseudomonas diminuta* for heterologous expression in *Escherichia coli* results in stabilization of the metal-free state. *Protein Eng. Des. Sel.* **18**, 51–58 (2005).
21. McLoughlin, S. Y., Jackson, C., Liu, J. W. & Ollis, D. Increased expression of a bacterial phosphotriesterase in *Escherichia coli* through directed evolution. *Protein Expr. Purif.* **41**, 433–440 (2005).
22. Caldwell, S. R., Newcomb, J. R., Schlecht, K. A. & Raushel, F. M. Limits of diffusion in the hydrolysis of substrates by the phosphotriesterase from *Pseudomonas diminuta*. *Biochemistry* **30**, 7438–7444 (1991).
23. Hong, S. B. & Raushel, F. M. Metal–substrate interactions facilitate the catalytic activity of the bacterial phosphotriesterase. *Biochemistry* **35**, 10904–10912 (1996).
24. Naqvi, T. et al. A 5,000-fold increase in the specificity of a bacterial phosphotriesterase for malathion through combinatorial active site mutagenesis. *PLoS ONE* **9**, e94177 (2014).
25. Benning, M. M., Kuo, J. M., Raushel, F. M. & Holden, H. M. Three-dimensional structure of phosphotriesterase: an enzyme capable of detoxifying organophosphate nerve agents. *Biochemistry* **33**, 15001–15007 (1994).
26. Singh, B. K. Organophosphorus-degrading bacteria: ecology and industrial applications. *Nat. Rev. Microbiol.* **7**, 156–164 (2009).
27. Sogorb, M. A., Vilanova, E. & Carrera, V. Future applications of phosphotriesterases in the prophylaxis and treatment of organophosporus insecticide and nerve agent poisonings. *Toxicol. Lett.* **151**, 219–233 (2004).
28. Yang, C. Y. et al. Improved stability and half-life of fluorinated phosphotriesterase using rosetta. *ChemBioChem* **15**, 1761–1764 (2014).
29. Rochu, D. et al. Contribution of the active-site metal cation to the catalytic activity and to the conformational stability of phosphotriesterase: temperature- and pH-dependence. *Biochem. J.* **380**, 627–633 (2004).
30. Chen-Goodspeed, M., Sogorb, M. A., Wu, F. Y., Hong, S. B. & Raushel, F. M. Structural determinants of the substrate and stereochemical specificity of phosphotriesterase. *Biochemistry* **40**, 1325–1331 (2001).
31. Jackson, C. J. et al. Structure-based rational design of a phosphotriesterase. *Appl. Environ. Microbiol.* **75**, 5153–5156 (2009).
32. Pavelka, A., Chovancova, E. & Damborsky, J. Hotspot wizard: a web server for identification of hot spots in protein engineering. *Nucleic Acids Res.* **37**, W376–W383 (2009).
33. Olsen, A. J. et al. Impact of phenylalanines outside the dimer interface on phosphotriesterase stability and function. *Mol. Biosyst.* **13**, 2092–2106 (2017).
34. Baker, P. J. & Montclare, J. K. Enhanced refoldability and thermoactivity of fluorinated phosphotriesterase. *ChemBioChem* **12**, 1845–1848 (2011).
35. Malone, L. A., Burgess, E. P. J., Stefanovic, D. & Gatehouse, H. S. Effects of four protease inhibitors on the survival of worker bumblebees, *Bombus terrestris L. Apidologie* **31**, 25–38 (2000).
36. Rademacher, E., Harz, M. & Schneider, S. Effects of oxalic acid on *Apis mellifera* (hymenoptera: apidae). *Insects* **8**, 84 (2017).
37. Bailey, L. The action of the proventriculus of the honeybee (*Apis mellifera L.*). *Bee World* **32**, 92 (1951).
38. Peng, Y. S. & Marston, J. M. Filtering mechanism of the honey bee proventriculus. *Physiol. Entomol.* **11**, 433–439 (1986).
39. Roth, R., Schoelkopf, J., Huwyler, J. & Puchkov, M. Functionalized calcium carbonate microparticles for the delivery of proteins. *Eur. J. Pharm. Biopharm.* **122**, 96–103 (2018).
40. Boyjoo, Y., Pareek, V. K. & Liu, J. Synthesis of micro and nano-sized calcium carbonate particles and their applications. *J. Mater. Chem. A* **2**, 14270–14288 (2014).
41. Song, J., Wang, R., Liu, Z. & Zhang, H. S. Preparation and characterization of calcium carbonate microspheres and their potential application as drug carriers. *Mol. Med. Rep.* **17**, 8403–8408 (2018).

42. Fu, M. F., Wang, A. H., Zhang, X. M., Dai, L. R. & Li, J. B. Direct observation of the distribution of gelatin in calcium carbonate crystals by super-resolution fluorescence microscopy. *Angew. Chem. Int. Ed.* **55**, 908–911 (2016).
43. Wszelaka-Rylik, M., Piotrowska, K. & Gierycz, P. Simulation, aggregation and thermal analysis of nanostructured calcite obtained in a controlled multiphase process. *J. Therm. Anal. Calorim.* **119**, 1323–1338 (2015).
44. Sukhorukov, G. B. et al. Porous calcium carbonate microparticles as templates for encapsulation of bioactive compounds. *J. Mater. Chem.* **14**, 2073–2081 (2004).
45. Griffiths, A. D. & Tawfik, D. S. Directed evolution of an extremely fast phosphotriesterase by in vitro compartmentalization. *EMBO J.* **22**, 24–35 (2003).
46. Bigley, A. N. & Raushel, F. M. Catalytic mechanisms for phosphotriesterases. *Biochim. Biophys. Acta* **1834**, 443–453 (2013).
47. Chen, Y. Z., Luo, Z. G. & Lu, X. X. Construction of novel enzyme–graphene oxide catalytic interface with improved enzymatic performance and its assembly mechanism. *ACS Appl. Mater. Interfaces* **11**, 11349–11359 (2019).
48. Li, P. et al. Nanosizing a metal–organic framework enzyme carrier for accelerating nerve agent hydrolysis. *ACS Nano* **10**, 9174–9182 (2016).
49. Wang, Y. et al. Rolling circle transcription-amplified hierarchically structured organic–inorganic hybrid RNA flowers for enzyme immobilization. *ACS Appl. Mater. Interfaces* **11**, 22932–22940 (2019).
50. Som, A. et al. Monodispersed calcium carbonate nanoparticles modulate local pH and inhibit tumor growth in vivo. *Nanoscale* **8**, 12639–12647 (2016).
51. Katyal, P., Chu, S. & Montclare, J. K. Enhancing organophosphate hydrolase efficacy via protein engineering and immobilization strategies. *Ann. N. Y. Acad. Sci.* https://doi.org/10.1111/nyas.14451 (2020).
52. Arena, M. & Sgolastra, F. A meta-analysis comparing the sensitivity of bees to pesticides. *Ecotoxicology* **23**, 324–334 (2014).
53. Al Naggar, Y. et al. Organophosphorus insecticides in honey, pollen and bees (*Apis mellifera L.*) and their potential hazard to bee colonies in Egypt. *Ecotoxicol. Environ. Saf.* **114**, 1–8 (2015).
54. Martin, M. M. & Lindqvist, L. The pH dependence of fluorescein fluorescence. *J. Lumin.* **10**, 381–390 (1975).
55. Cochran, R. in *Hayes' Handbook of Pesticide Toxicology* (ed. Krieger, R.) 337–355 (Elsevier, 2010).
56. Gradish, A. E. et al. Comparison of pesticide exposure in honey bees (hymenoptera: apidae) and bumble bees (hymenoptera: apidae): implications for risk assessments. *Environ. Entomol.* **48**, 12–21 (2019).
57. Peng, Y. S., Nasr, M. E. & Marston, J. M. Release of alfalfa, *Medicago sativa*, pollen cytoplasm in the gut of the honey bee, *Apis mellifera* (hymenoptera: apidae). *Ann. Entomol. Soc. Am.* **79**, 804–807 (1986).
58. Kroon, G., Van Praagh, J. & Velthuis, H. Osmotic shock as a prerequisite to pollen digestion in the alimentary tract of the worker honeybee. *J. Apic. Res.* **13**, 177–181 (1974).
59. Chaganti, L. K., Venkatakrishnan, N. & Bose, K. An efficient method for FITC labelling of proteins using tandem affinity purification. *Biosci. Rep.* **38**, BSR20181764 (2018).
60. Ellman, G. L., Courtney, K. D., Andres, V. & Featherstone, R. M. A new and rapid colorimetric determination of acetylcholinesterase activity. *Biochem. Pharmacol.* **7**, 88–95 (1961).

Acknowledgements

This material is based on work that are partially supported by the National Institute of Food and Agriculture, US Department of Agriculture, Hatch under 2017-18-107, Counter ACT Program of the National Institute of Health under Award Number R21-NS10383-01 and the National Science Foundation under Award Number IIP-1918981. This work made use of the Cornell Center for Materials Research Shared Facilities which are supported through the NSF MRSEC programme (DMR-1719875).

Author contributions

J.C. and M.M. conceived the study. J.C. and J.W. designed and conducted the experiments. S.G. and J.-K.M. provided the *E. coli* strain. K.S. drew the schemes. J.C., J.W., J.-K.M., S.M. and M.M. reviewed and interpreted the results. J.C, J.W. and M.M. wrote the manuscript, with input from all authors. All authors reviewed and commented on the manuscript.

Competing interests

The technology described in this paper is being licensed to Beemmunity Inc., a start-up company co-founded by J.W. M.M. and J.C. are scientific advisors and shareholders of Beemmunity Inc.

Additional information

Supplementary information The online version contains supplementary material available at https://doi.org/10.1038/s43016-021-00282-0.

Correspondence and requests for materials should be addressed to M.M.

Peer review information *Nature Food* thanks Liangfang Zhang, Scott Walper and Scott Medina for their contribution to the peer review of this work.

Reprints and permissions information is available at www.nature.com/reprints.

Publisher's note Springer Nature remains neutral with regard to jurisdictional claims in published maps and institutional affiliations.

nature research

Corresponding author(s): Minglin Ma

Last updated by author(s): Oct 21, 2020

Reporting Summary

Nature Research wishes to improve the reproducibility of the work that we publish. This form provides structure for consistency and transparency in reporting. For further information on Nature Research policies, see our Editorial Policies and the Editorial Policy Checklist.

Statistics

For all statistical analyses, confirm that the following items are present in the figure legend, table legend, main text, or Methods section.

n/a	Confirmed	
☐	☒	The exact sample size (*n*) for each experimental group/condition, given as a discrete number and unit of measurement
☐	☒	A statement on whether measurements were taken from distinct samples or whether the same sample was measured repeatedly
☐	☒	The statistical test(s) used AND whether they are one- or two-sided *Only common tests should be described solely by name; describe more complex techniques in the Methods section.*
☒	☐	A description of all covariates tested
☒	☐	A description of any assumptions or corrections, such as tests of normality and adjustment for multiple comparisons
☐	☒	A full description of the statistical parameters including central tendency (e.g. means) or other basic estimates (e.g. regression coefficient) AND variation (e.g. standard deviation) or associated estimates of uncertainty (e.g. confidence intervals)
☐	☒	For null hypothesis testing, the test statistic (e.g. *F*, *t*, *r*) with confidence intervals, effect sizes, degrees of freedom and *P* value noted *Give P values as exact values whenever suitable.*
☒	☐	For Bayesian analysis, information on the choice of priors and Markov chain Monte Carlo settings
☒	☐	For hierarchical and complex designs, identification of the appropriate level for tests and full reporting of outcomes
☒	☐	Estimates of effect sizes (e.g. Cohen's *d*, Pearson's *r*), indicating how they were calculated

Our web collection on statistics for biologists contains articles on many of the points above.

Software and code

Policy information about availability of computer code

Data collection	Microparticle morphology were observed with an evos FL microscope and a zeiss gemini 500 scanning electron microscope. Pore size distribution was determined with an ASAP 2460 micromeritics. Microparticles suspension ability was determined with an eppendorf BioPhotometer. All CLSM images was obtained with a Zeiss 710 confocal microscope. All UV absorptions were obtained with BioTek plate reader.
Data analysis	All statistical analyses were performed on Graphpad Prism (version 7). All the microparticle images was analyzed with ImageJ software (64-bit Java 1.8.0_172).

For manuscripts utilizing custom algorithms or software that are central to the research but not yet described in published literature, software must be made available to editors and reviewers. We strongly encourage code deposition in a community repository (e.g. GitHub). See the Nature Research guidelines for submitting code & software for further information.

Data

Policy information about availability of data

All manuscripts must include a data availability statement. This statement should provide the following information, where applicable:

- Accession codes, unique identifiers, or web links for publicly available datasets
- A list of figures that have associated raw data
- A description of any restrictions on data availability

The main data supporting the results in this study are available within the paper and its Supplementary Information. The raw and analysed datasets generated during the study are too large to be publicly shared, yet they are available for research purposes from the corresponding authors on reasonable request.

Field-specific reporting

Please select the one below that is the best fit for your research. If you are not sure, read the appropriate sections before making your selection.

☒ Life sciences ☐ Behavioural & social sciences ☐ Ecological, evolutionary & environmental sciences

For a reference copy of the document with all sections, see nature.com/documents/nr-reporting-summary-flat.pdf

Life sciences study design

All studies must disclose on these points even when the disclosure is negative.

Sample size	For the in vitro and in vivo experiments, we followed the standards for good scientific practice. We used at least 3 biological replicates per group, to calculate means and standard deviations and to perform statistical analyses.
Data exclusions	No data were excluded.
Replication	Each experiment was replicated multiple times, and the replication numbers are listed both in 'Methodology' and below each figure. Replicates were reproducible.
Randomization	All samples and organisms were randomly allocated into experimental groups.
Blinding	No formal blinding was used. The survival study was conducted by an independent operator, who was unaware of the treatment conditions.

Reporting for specific materials, systems and methods

We require information from authors about some types of materials, experimental systems and methods used in many studies. Here, indicate whether each material, system or method listed is relevant to your study. If you are not sure if a list item applies to your research, read the appropriate section before selecting a response.

Materials & experimental systems

n/a	Involved in the study
☒	☐ Antibodies
☐	☒ Eukaryotic cell lines
☒	☐ Palaeontology and archaeology
☐	☒ Animals and other organisms
☒	☐ Human research participants
☒	☐ Clinical data
☒	☐ Dual use research of concern

Methods

n/a	Involved in the study
☒	☐ ChIP-seq
☒	☐ Flow cytometry
☒	☐ MRI-based neuroimaging

Eukaryotic cell lines

Policy information about cell lines

Cell line source(s)	Apis melifera (honey bees) cell membrane.
Authentication	Apis melifera (honey bees) were acquired from colonies of the McArt Lab at Cornell.
Mycoplasma contamination	No mycoplasma contamination was found.
Commonly misidentified lines (See ICLAC register)	No commonly misidentified cell lines were used.

Animals and other organisms

Policy information about studies involving animals; ARRIVE guidelines recommended for reporting animal research

Laboratory animals	B. impatiens (bumble bees) were acquired from Biobest. Apis melifera (honey bees) were acquired from colonies of the McArt Lab at Cornell.
Wild animals	The study did not involve wild animals.
Field-collected samples	The study did not involve samples collected from the field.

Ethics oversight	All animal studies were approved by the Cornell Institutional Animal Care and Use Committee.

Note that full information on the approval of the study protocol must also be provided in the manuscript.